Distributed DAE Modelling of Feeders with High Penetration of IBRs

Freeman Martin, Georgios Tzounas, *IEEE Member*

***Abstract*— This paper develops a continuum-based model for steady-state analysis of distribution feeders with high penetration of inverter-based resources (IBRs). The model is derived from Kirchhoff's laws and describes the spatial evolution of voltage magnitude, phase, and power flows along distribution feeders while representing IBR injections and loads through a composite formulation that combines constant-power, constant-current, and constant-current-density behaviours, referred to as JIP model. Analytical results for a DC feeder reveal a formal analogy with the Euler–Bernoulli beam equation, and AC case studies demonstrate the impact of different injection and load profiles.**

***Index Terms*— Continuum modelling, active distribution networks, inverter-based resources (IBRs), mechanical analogies.**

I. Introduction

A. Motivation

Distribution networks are evolving from passive grids with unidirectional power flows to active networks that integrate a growing number of electronic inverter-based renewable sources, energy storage devices and flexible loads. The growing complexity of these networks poses several challenges to their modelling and analysis. This paper departs from standard lumped-node approaches and investigates the potential of a continuum-based representation of voltage variations and power flows along active distribution feeders that integrate numerous inverter-based resources (IBRs).

B. Literature Review

The underlying motivation for treating a system of lumped elements as a continuum is the potential to gain insight through simplified analysis. This idea is standard in other fields. For example, matter is composed of discrete particles, yet tracking their individual behaviours in complex mechanical systems is often impractical. Instead, treating matter as a continuous field enables analysis of the macroscale behaviour of structures and fluids [1]–[3], such as their elastic/plastic deformation under various loading conditions.

In power systems, the idea of continuum-based modelling was first explored through the so-called electromechanical wave approach [4]–[6]. Therein, synchronous machines were represented as a continuous distribution along transmission lines to capture the propagation of power disturbances. Later works explored variations of the same concept in more general network settings, e.g., see [6]–[8]. However, a key requirement for a continuum abstraction to hold is the presence of a high density of lumped elements, whereas real-world transmission networks typically contain few synchronous machines that are electrically dispersed. This makes it difficult to distribute them without losing critical information [9]. For this reason, the above approach achieved only limited success.

A continuum-based modelling approach is particularly better suited for modern distribution networks that integrate large amounts of IBRs. In such settings, traditional lumped models may become cumbersome to analyse [10], [11], while detailed data for every device may often not even be available. By treating distribution feeders as a continuous medium, techniques from field theory can be applied to produce insightful approximations of spatially varying voltage profiles. Such studies can become increasingly relevant as modern feeders exhibit strong coupling between bidirectional active power flows and voltage due to high R/X ratios, the proximity of voltage-dependent loads and the presence of controlled IBRs [12], [13]. Nevertheless, the application of continuum modelling to distribution networks has so far remained limited. Preliminary works have explored its potential for steady-state analysis. In this vein, a continuous formulation of the power flow equations is described in [14]. The model is used to study long feeders and to examine how spatial variability in consumption and generation affects voltage deviations as the feeder approaches its loadability limit. Moreover, [15] incorporates IBR voltage–reactive power (v – Q) controllers into a continuum formulation to analyse voltage stability in long PV-rich feeders. Finally, the behaviour of spatially distributed electric vehicle (EV) charging stations, including the impact of different charging/discharging power injection profiles on feeder voltage profiles, is discussed in [16], [17].

C. Contribution

This paper develops a continuum model for steady-state analysis of distribution feeders with high penetration of IBRs. The model incorporates a composite injection scheme that represents constant-power, constant-current, and constant-current-density behaviours of distributed resources and loads. Analytical results for a DC feeder reveal a formal analogy with the Euler–Bernoulli beam equation, providing intuitive physical insight and complementing the numerical case studies.

D. Organization

The remainder of this paper is organised as follows. Section II introduces the continuum model formulation, deriving the governing equations, injection model, and explains the computational methods. Section III presents analytical insights, including the DC feeder special case and its mechanical analogy. Numerical simulation results for more complex AC cases are presented in Section IV. Finally, conclusions are drawn and future work is discussed in Section V.

II. Continuum Model Formulation

A. Governing Equations

We consider a distribution feeder with IBRs and loads connected along its length. To describe the feeder's spatial behaviour, we examine a small segment between positions x and $x+\Delta x$, as illustrated in Fig. 1, where Δx represents the distance between injection nodes aggregating connected IBRs and loads. The series impedance of the segment is denoted as $\Delta\bar{Z}$. The voltage and current phasors at the endpoints of the segment are denoted as $\bar{v}(x)$, $\bar{v}(x+\Delta x)$ and $\bar{\imath}(x)$, $\bar{\imath}(x+\Delta x)$, respectively. Applying Kirchhoff's laws, the change in current and voltage across the segment are:

$$\bar{\imath}(x+\Delta x)-\bar{\imath}(x)=\Delta\bar{\imath}(x) \tag{1}$$

$$\bar{v}(x+\Delta x)-\bar{v}(x)=-\Delta\bar{Z}\,[\bar{\imath}(x)+\Delta\bar{\imath}(x)] \tag{2}$$

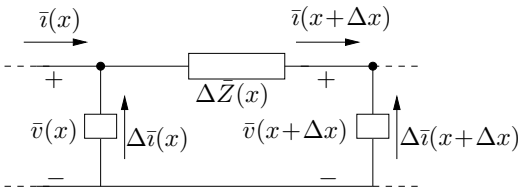

Fig. 1: Segment of active distribution feeder.

By dividing (1), (2) by Δx and taking the limit of infinitesimal IBR spacing, we obtain the continuum model:

$$d\bar{\imath}(x)/dx=\bar{J}(x) \tag{3}$$

$$d\bar{v}(x)/dx=-\bar{z}\,\bar{\imath}(x) \tag{4}$$

where $\bar{z}=d\bar{Z}/dx$ is the per-unit-length series impedance at x; and $\bar{J}(x)$ is the net current injection density, where:

$$\bar{J}(x)=\bar{J}_G(x)-\bar{J}_D(x)$$

with $\bar{J}_G(x)$ and $\bar{J}_D(x)$ being, respectively, the current densities of power generation and consumption at x.

B. Variation of Voltage Magnitude and Phase

Let us express the voltage phasor at x as $\bar{v}=v\angle\theta$, where $v=v(x)$ and $\theta=\theta(x)$ are the voltage magnitude and phase angle, respectively; and the current phasor as $\bar{\imath}=\bar{\imath}_P+\jmath\bar{\imath}_Q$, where $\bar{\imath}_P=\bar{\imath}_P(x)$ and $\bar{\imath}_Q=\bar{\imath}_Q(x)$ are the active and reactive components of the current, respectively. Substituting into (4), we obtain:

$$e^{\jmath\theta}\Big(\frac{dv}{dx}+\jmath v\frac{d\theta}{dx}\Big)=-(r\imath_P-\chi\imath_Q)-\jmath(\chi\imath_P+r\imath_Q) \tag{5}$$

where r and χ are the resistance and reactance, respectively, per unit length, with $\bar{z}=r+\jmath\chi$. Separating real and imaginary parts in (5) yields:

$$dv/dx=-(r\imath_P-\chi\imath_Q)\cos\theta-(\chi\imath_P+r\imath_Q)\sin\theta \tag{6}$$

$$d\theta/dx=[(r\imath_P-\chi\imath_Q)\sin\theta-(\chi\imath_P+r\imath_Q)\cos\theta]/v \tag{7}$$

where the explicit dependence on x is omitted for brevity. To further simplify (6)-(7), we transform the current components into a rotated frame where one component is aligned with the line impedance and the other is orthogonal to it in the complex plane [18], as follows:

$$\imath_p=(r\imath_P-\chi\imath_Q)/z\ ,\qquad \imath_q=(\chi\imath_P+r\imath_Q)/z \tag{8}$$

where $z=\sqrt{r^2+\chi^2}$. In matrix form:

$$\begin{bmatrix}\imath_p\\ \imath_q\end{bmatrix}=\begin{bmatrix}r/z & -\chi/z\\ \chi/z & r/z\end{bmatrix}\begin{bmatrix}\imath_P\\ \imath_Q\end{bmatrix}=\begin{bmatrix}\cos\beta & -\sin\beta\\ \sin\beta & \cos\beta\end{bmatrix}\begin{bmatrix}\imath_P\\ \imath_Q\end{bmatrix} \tag{9}$$

where $\beta=\arctan(\chi/r)$. Substituting (8) into (6)-(7), we obtain the following expressions for the spatial evolution of voltage magnitude and phase across the distribution feeder:

$$dv/dx=-z\imath_p\cos\theta-z\imath_q\sin\theta \tag{10}$$

$$d\theta/dx=(z\imath_p\sin\theta-z\imath_q\cos\theta)/v \tag{11}$$

C. Variation of Active and Reactive Power

Let us express the complex power flow $\bar{S}(x)$ at x as follows:

$$\bar{S}(x)=\bar{v}(x)\bar{\imath}^*(x)=P(x)+\jmath Q(x) \tag{12}$$

where $*$ denotes the complex conjugate. Differentiating with respect to x gives:

$$\frac{d\bar{S}}{dx}=\bar{\imath}^*\frac{d\bar{v}}{dx}+\bar{v}\frac{d\bar{\imath}^*}{dx}=-\bar{z}\imath^2+\bar{v}\bar{J}^* \tag{13}$$

In (13), the first term, $-\bar{z}\imath^2$, represents the variation of power flow due to the series impedance, while the second term, $\bar{v}\bar{J}^*$, accounts for the contribution from the power injection of IBRs and loads at x. The second term can be written as:

$$\bar{v}\bar{J}^*=\frac{dP^{\mathrm{inj}}}{dx}+\jmath\frac{dQ^{\mathrm{inj}}}{dx} \tag{14}$$

with

$$\begin{aligned}dP^{\mathrm{inj}}/dx&=vJ_P\cos\theta+vJ_Q\sin\theta\\ dQ^{\mathrm{inj}}/dx&=vJ_Q\cos\theta-vJ_P\sin\theta\end{aligned} \tag{15}$$

where $\bar{J}=J_P+\jmath J_Q$.

D. Distributed Current Density Model

We introduce a composite model for IBRs and loads that combines constant power density, constant current, and constant current density behaviours. Accordingly, the current injection density at x is expressed as:

$$\begin{aligned}J_P&=J_{P\mathrm{P}}+J_{P\mathrm{I}}+J_{P\mathrm{J}}\\ J_Q&=J_{Q\mathrm{P}}+J_{Q\mathrm{I}}+J_{Q\mathrm{J}}\end{aligned} \tag{16}$$

Splitting the real and imaginary parts in (3), we obtain:

$$d\imath_P/dx=J_P\ ,\qquad d\imath_Q/dx=J_Q$$

From the solution of (15), J_P and J_Q can be written as:

$$\begin{aligned}J_P&=\frac{1}{v}\left(\frac{dP^{\mathrm{inj}}}{dx}\cos\theta+\frac{dQ^{\mathrm{inj}}}{dx}\sin\theta\right)\\ J_Q&=\frac{1}{v}\left(\frac{dQ^{\mathrm{inj}}}{dx}\cos\theta-\frac{dP^{\mathrm{inj}}}{dx}\sin\theta\right)\end{aligned} \tag{17}$$

In the following, we describe the expression of each component in (16).

1) Constant Power Density: For a constant power injection density model, we have $dP^{\rm inj}(x)/dx = P_{d\rm P} = \text{const.}$ and $dQ^{\rm inj}(x)/dx = Q_{d\rm P} = \text{const.}$ Using (17), the expressions of $J_{P\rm P}$ and $J_{Q\rm P}$ in (16) are:

$$\begin{aligned} J_{P\rm P} &= \left(P_{d\rm P}\cos\theta + Q_{d\rm P}\sin\theta\right)/v \\ J_{Q\rm P} &= \left(Q_{d\rm P}\cos\theta - P_{d\rm P}\sin\theta\right)/v \end{aligned} \tag{18}$$

2) Constant Current: For a constant current model, the active and reactive power injections vary linearly with voltage magnitude. Thus, $dP^{\rm inj}/dx = P_{\rm I}^{\rm inj} dv/dx$ and $dQ^{\rm inj}/dx = Q_{\rm I}^{\rm inj} dv/dx$, where $P_{\rm I}^{\rm inj}$ and $Q_{\rm I}^{\rm inj}$ are constant coefficients. The expressions of $J_{P\rm I}$ and $J_{Q\rm I}$ in (16) are:

$$\begin{aligned} J_{P\rm I} &= (P_{\rm I}^{\rm inj} E\cos\theta + Q_{\rm I}^{\rm inj} E\sin\theta)/v \\ J_{Q\rm I} &= (Q_{\rm I}^{\rm inj} E\cos\theta - P_{\rm I}^{\rm inj} E\sin\theta)/v \end{aligned} \tag{19}$$

where $E(x) = dv/dx = -z\imath_p\cos\theta - z\imath_q\sin\theta$.

3) Constant Current Density: In the constant current density model, the injection profiles $J_{P\rm J}$ and $J_{Q\rm J}$ in (16) are given directly as voltage-independent functions of x:

$$J_{P\rm J} = J_{P\rm J}(x)\,, \qquad J_{Q\rm J} = J_{Q\rm J}(x) \tag{20}$$

We will refer to (16) as the JIP model.

E. Complete Model

Combining the above expressions yields a differential-algebraic system with four state variables and nine algebraic variables. The column vectors of state variables ($\mathbf{x}$) and algebraic variables ($\mathbf{y}$) are defined as:

$$\mathbf{x} = [\imath_P\ \imath_Q\ v\ \theta]^\intercal,\ \mathbf{y} = [\imath_p\ \imath_q\ E\ J_P\ J_Q\ J_{P\rm P}\ J_{Q\rm P}\ J_{P\rm I}\ J_{Q\rm I}]^\intercal$$

The differential equations are:

$$d\imath_P/dx = J_P \tag{21}$$
$$d\imath_Q/dx = J_Q \tag{22}$$
$$dv/dx = E \tag{23}$$
$$d\theta/dx = (z\imath_p\sin\theta - z\imath_q\cos\theta)/v \tag{24}$$

The corresponding algebraic constraints are:

$$0 = \imath_p - (r\imath_P - \chi\imath_Q)/z \tag{25}$$
$$0 = \imath_q - (\chi\imath_P + r\imath_Q)/z \tag{26}$$
$$0 = E + z\imath_p\cos\theta + z\imath_q\sin\theta \tag{27}$$
$$0 = J_P - J_{P\rm P} - J_{P\rm I} - J_{P\rm J} \tag{28}$$
$$0 = J_Q - J_{Q\rm P} - J_{Q\rm I} - J_{Q\rm J} \tag{29}$$
$$0 = J_{P\rm P} - \left(P_{d\rm P}\cos\theta + Q_{d\rm P}\sin\theta\right)/v \tag{30}$$
$$0 = J_{Q\rm P} - \left(Q_{d\rm P}\cos\theta - P_{d\rm P}\sin\theta\right)/v \tag{31}$$
$$0 = J_{P\rm I} - (P_{\rm I}^{\rm inj} E\cos\theta + Q_{\rm I}^{\rm inj} E\sin\theta)/v \tag{32}$$
$$0 = J_{Q\rm I} - (Q_{\rm I}^{\rm inj} E\cos\theta - P_{\rm I}^{\rm inj} E\sin\theta)/v \tag{33}$$

In total, the system contains 13 variables and 13 equations. The model variables and parameters are summarized in Table I. Note that the model is non-autonomous and it becomes autonomous if and only if all parameters are assumed to be constant along the feeder.

TABLE I: Continuum model: variables and parameters.

Type	List	Total number
State variables	$\imath_P$, $\imath_Q$, v, θ	4
Algebraic variables	$\imath_p$, $\imath_q$, E, J_P, J_Q, $J_{P\rm P}$, $J_{Q\rm P}$, $J_{P\rm I}$, $J_{Q\rm I}$,	9
Parameters	r, χ, $P_{d\rm P}$, $Q_{d\rm P}$, $P_{\rm I}^{\rm inj}$, $Q_{\rm I}^{\rm inj}$, $J_{P\rm J}$, $J_{Q\rm J}$	8

F. Boundary Conditions and Numerical Solution

The solution of (21)–(33) constitutes a boundary value problem and requires the specification of appropriate boundary conditions. In our case, well-posedness requires four independent boundary conditions, corresponding to the order of the model. As an example, let us consider the case where the voltage magnitude and angle are fixed at one end of the feeder ($x = 0$), while the other end ($x = L$, where L is the line length) is open. The corresponding boundary conditions are:

$$v(0) = v_0\ ,\ \theta(0) = \theta_0\ ,\ \imath_P(L) = 0\ ,\ \imath_Q(L) = 0$$

These conditions imply the following boundary values for the algebraic variables:

$$\begin{aligned} &\imath_p(L)=0\,,\ \imath_q(L)=0\,,\ E(L)=0\,,\ J_P(L)=0, J_Q(L)=0, \\ &J_{P\rm I}(L)=0\,,\ J_{Q\rm I}(L)=0\,, \\ &J_{P\rm P}(0) = \left[P_{d\rm P}(0)\cos\theta_0 + Q_{d\rm P}(0)\sin\theta_0\right]/v_0 \\ &J_{Q\rm P}(0) = \left[Q_{d\rm P}(0)\cos\theta_0 - P_{d\rm P}(0)\sin\theta_0\right]/v_0 \end{aligned}$$

To solve the boundary value problem defined by (21)–(33), one can employ a shooting method [19]. This approach transforms the problem into an equivalent initial value problem, which is numerically more tractable. The idea is to use the known initial values at $x = 0$, guess the remaining ones, and numerically integrate the system forward up to $x = L$. The result is then compared against the desired terminal conditions, and the process is repeated iteratively until convergence is achieved. Each integration from $x = 0$ to L is performed in this paper using the trapezoidal method, while the iterative update of initial conditions is carried out using Newton's method.

Consider the case discussed in Section II-F, where $v(0)$, $\theta(0)$ are known and $\imath_P(0)$ and $\imath_Q(0)$ are unknown. Let $\imath_P^{[k]}(0)$ and $\imath_Q^{[k]}(0)$ denote the guesses at the k-th iteration of the process. After integrating the system, we obtain terminal values $\imath_P^{[k]}(L)$ and $\imath_Q^{[k]}(L)$, which are compared to the desired boundary values $\imath_P(L) = 0$ and $\imath_Q(L) = 0$. The corresponding shooting error is:

$$\boldsymbol{\epsilon}^{[k]} = \begin{bmatrix} \imath_P^{[k]}(L) - \imath_P(L) \\ \imath_Q^{[k]}(L) - \imath_Q(L) \end{bmatrix}$$

The initial values are then refined as follows:

$$\begin{bmatrix} \imath_P^{[k+1]}(0) \\ \imath_Q^{[k+1]}(0) \end{bmatrix} = \begin{bmatrix} \imath_P^{[k]}(0) \\ \imath_Q^{[k]}(0) \end{bmatrix} - (\mathbf{J}^{[k]})^{-1}\boldsymbol{\epsilon}^{[k]}$$

where $\mathbf{J}^{[k]}$ is the Jacobian matrix of the shooting error with respect to the initial conditions:

$$\mathbf{J}^{[k]} = \begin{bmatrix} \partial \imath_P^{[k]}(L)/\partial \imath_P^{[k]}(0) & \partial \imath_P^{[k]}(L)/\partial \imath_Q^{[k]}(0) \\ \partial \imath_Q^{[k]}(L)/\partial \imath_P^{[k]}(0) & \partial \imath_Q^{[k]}(L)/\partial \imath_Q^{[k]}(0) \end{bmatrix}$$

III. Analytical Results

A. Mechanical Analogy of DC Feeder

Using the notation $v = d\psi/dx$, (4) can be written as:

$$d^3\psi/dx^3 = rJ_P \tag{34}$$

and thus:

$$d^4\psi/dx^4 = rdJ_P/dx \tag{35}$$

Note the straight analogy of the last equation with the Euler–Bernoulli Beam Equation [3]:

$$\frac{d^4y}{dx^4} = \frac{1}{\mathcal{E}I} f \tag{36}$$

where $\mathcal{E}I$ is the beam flexural rigidity; y is the vertical displacement; and f is the distributed force applied to the beam. The analogy is summarized in Table II.

TABLE II: Analogy of DC feeder with mechanical beam.

Electrical quantity	Mechanical quantity
Voltage integral $\psi(x)$	Vertical displacement $y(x)$
Voltage $v(x)$	Deflection angle $\alpha(x)$
Line current $\imath_P(x)$	Bending moment $M(x)$
Current density $J_P(x)$	Shear force $F(x) = \mathcal{E}Id^3y(x)/dx^3$
$dJ_P(x)/dx$	Distributed force $f(x) = dF(x)/dx$
Conductance per unit length $1/r$	Flexural rigidity $\mathcal{E}I$

For the sake of illustration, assume that the DC line has a linearly varying current density, that is $J_P = J_{P\mathrm{J}}$. This case is formally analogous to a beam with uniform distributed force f.

B. Analytical Results for a DC Feeder

The boundary conditions discussed in Section II-F are applied. As this is a simple case study an analytical expression can be derived. Integrating (3), and taking into account that $\bar{J}(x) = \bar{J}$ is constant, we get:

$$\begin{aligned} \int_x^L d\bar{\imath} &= \int_x^L \bar{J}(l)dl \\ \Rightarrow \bar{\imath}(x) &= -\bar{J}(L-x) = -\bar{J}L + \bar{J}x \end{aligned} \tag{37}$$

Integrating (4) with respect to x, we get:

$$\int_0^x d\bar{v} = -\int_0^x \bar{z}\,\bar{\imath}(l)dl \Rightarrow \bar{v}(x) = \bar{v}_0 - \bar{z}\bar{J}Lx + \frac{\bar{z}\bar{J}}{2}x^2 \tag{38}$$

IV. Numerical Simulations

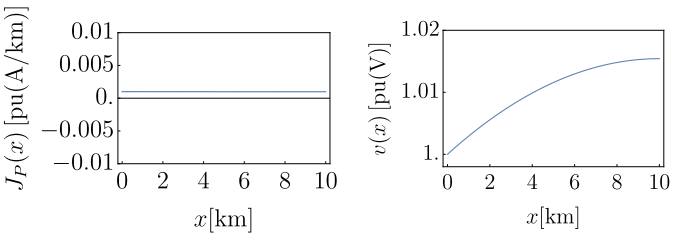

(a) Current injection profile (b) Voltage profile

Fig. 2: DC feeder under constant current injection

As shown in Fig. 2a, the active current injections are constant along the line. This produces a concave-downward voltage profile, the voltage rises quadratically along the length of the cable. This result matches the form of the analytically derived voltage equation (38).

A. AC Feeder

The same system can be extended to an AC system with a constant power load model. The phase angle of the current injections ϕ is varied such that $\phi \in \{0°, 45°, 90°\}$, in order to compare the behaviour of active, reactive, and complex current injections.

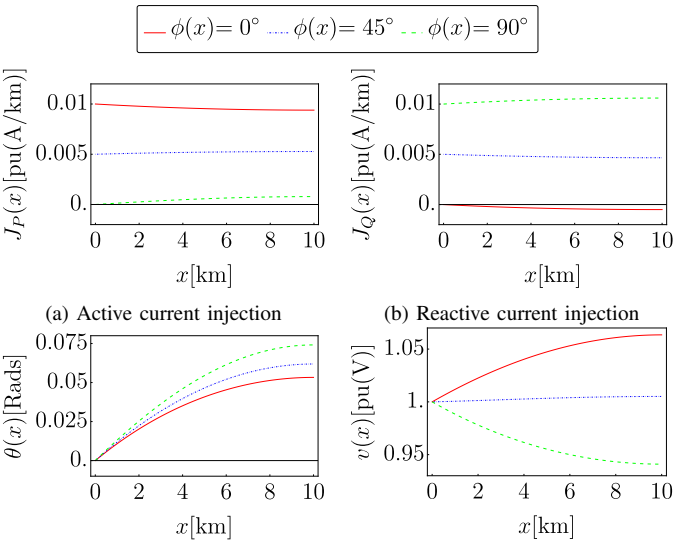

(a) Active current injection (b) Reactive current injection

(c) Voltage angle. (d) Voltage magnitude.

Fig. 3: AC feeder voltage under different injection phase angles.

The results in Fig. 3 highlight the effect of the different injection profiles shown in Fig. **??**. When $\phi = 0°$, the active power injections create an increase in the voltage magnitude and phase. For $\phi = 90°$, reactive injection dominates, this results in the largest increase in the voltage phase and a decrease in the voltage magnitude. Finally, the mixed injections produce an increase in the voltage phase at an intermediate rate. The voltage magnitude remained almost flat. The effects of the active and reactive injections oppose each other resulting in no net change.

1) JIP Modelling: This study analyses the behaviour of a distribution feeder with various load modelling approaches, constant power J_{PP} and constant current J_{PI}. Specifically, 3 scenarios are examined, using purely constant power, purely constant current, and a composite model that uses an equal linear combination of both. The objective is to understand the effects different load models have on the system.

The voltage is fixed at the sending end, such that $v(0) = 1$ pu and $\theta(0) = 0$ Rads. The current is fixed at the receiving end, such that $\imath_P(L) = 0$ pu and $\imath_Q(L) = 0$ pu.

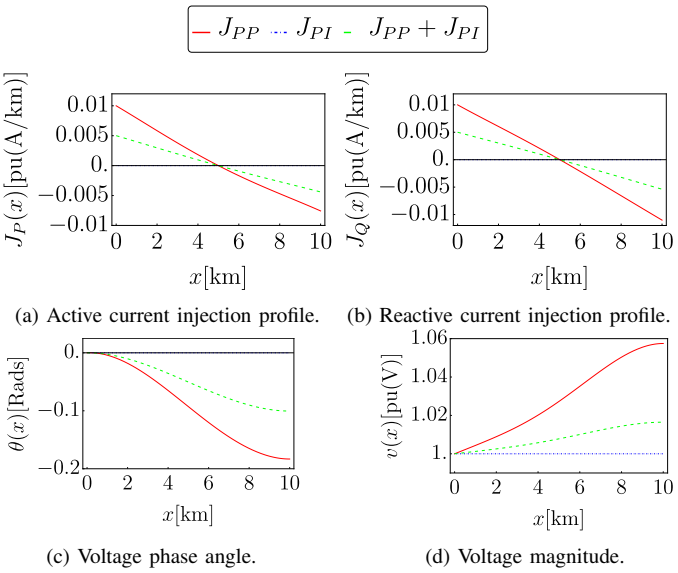

(a) Active current injection profile. (b) Reactive current injection profile.

(c) Voltage phase angle. (d) Voltage magnitude.

Fig. 4: Impact of different load models on voltage along AC feeder.

The current injection profiles shown in Figs. 4a and 4b show the differences between the load models. The constant power model results in a significant variation in active and reactive injections along the line. This reflects the sensitivity of this model to local voltage variations. In contrast, the constant current model exhibits negligible injections along the line. This behaviour is expected given the equations depend on the spatial voltage gradient, which remains small under typical operating conditions. Consequently, the composite model is dominated by the constant power component.

The voltage magnitude and phase for the constant current model remain unchanged across the length of the feeder, as expected. In the composite and constant power models the voltage magnitude increases along the feeder indicating the line has a net capacitive effect. The phase decreases along the line as a result of line losses and the net loading in the second half of the feeder.

2) Cloud: Next, a temporal disturbance was examined by introducing a parameter t.

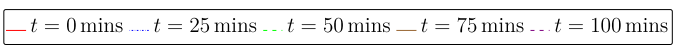

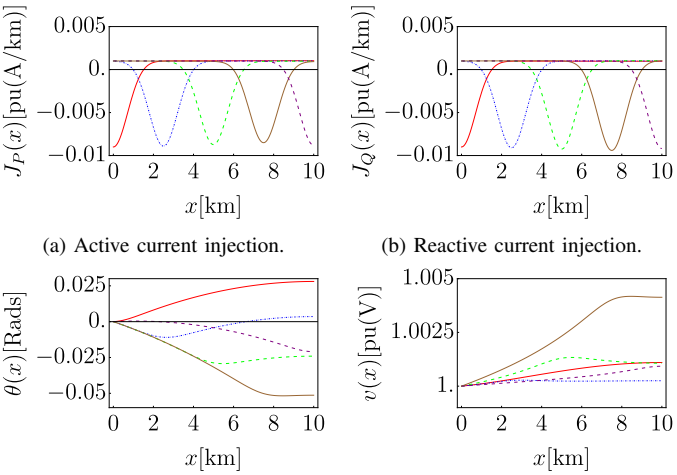

(a) Active current injection. (b) Reactive current injection.

(c) Voltage phase angle. (d) Voltage magnitude.

Fig. 5: Impact of moving cloud on the voltage along a PV-rich feeder.

Finally, a temporal disturbance was introduced to emulate the effects of a cloud passing over an area of high PV density. This injection profile was modelled using a Gaussian that is parametrised with respect to t, the resulting injection profiles are shown in Figs. 5a and 5b resulting voltage responses are shown in Fig. 5d and 5c. The voltage magnitude and phase exhibited localised variations corresponding to the spatial location of the disturbance. These results demonstrate the model's ability to capture spatially and temporally varying behaviours from intermittent IBR output, such as PV fluctuations due to moving clouds.

3) Cloud with control scheme: The same case with a cloud is examined but using a reactive current control scheme which aims to regulate $v(x) = 1$ pu, such that $Q_{dP}(x) = q_0 \tanh\left[(2(v(x) - 1))/\delta\right]$, where q_0 defines the magnitude of the controller response, and δ defines the steepness of the control curve. Applying this new condition to the system and comparing it to the uncontrolled results, we see that the maximum deviations in voltage magnitude are significantly reduced. This demonstrates the effectiveness of reactive current control in stabilising voltages under cloud-induced disturbances.

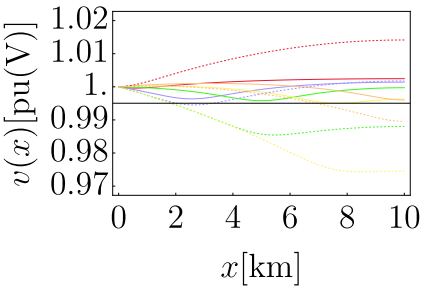

Fig. 6: Controlled vs uncontrolled voltage response to cloud.

4) Stochastic Cloud with Monte Carlo: Due to the stochastic nature of the weather, the cloud can be modelled using mean reverting stochastic differential equations. The parameters of this system can be sampled through Monte Carlo

simulations to examine a variety of speeds, widths, and amplitudes for the disturbance. The probabilities of an over/under voltage event occurring at any point along the feeder can be calculated using these simulations as a sample data set. This probabilistic analysis helps risk assessment, identification of vulnerable points on the feeder, and determine safe limits for DER penetration.

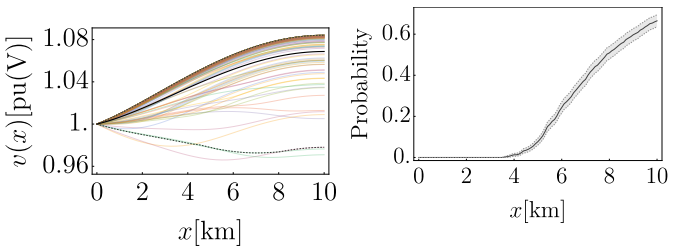

(a) Monte Carlo simulation of cloud parameters.

(b) Probability of voltage violations, 95% confidence interval.

Fig. 7: Monte Carlo study of cloud-induced voltage behaviour: (a) sampled cloud parameters; (b) spatial probability of over/under-voltage with 95% CI.

5) Stochastic Cloud with Markov chain forecasts:

V. Conclusion

This paper develops a continuum model for quasi-steady-state behaviour of distribution feeders with high penetration of inverter-based resources. The resulting model describes the spatial variations of voltages through a system of differential algebraic equations utilizing a generalized injection model that incorporates constant power, current, and current density load behaviours. The continuum formulation provides a method to create approximations of voltage levels in low visibility areas. Future work will focus on extending the model to include temporal dynamics, non-uniform parameters, and uncertainty in the system parameters.

VI. Appendix

TABLE III: Simulation parameters SAMPLE VALUES REMEMBER TO CHANGE

Parameter Type	Description	Value
V_{base}	Voltage base [V]	400.0
S_{base}	Power base [VA]	500 000.0
Z_{base}	Impedance base [Ω]	$V_{\text{base}}^2/S_{\text{base}}$
L	Feeder length [km]	10.0
r	Per-unit resistance	Computed from Z_{base}
χ	Per-unit reactance	Same as r
P_0, Q_0	Nominal load [pu]	0.009
v_μ	OU mean speed [km/unit time]	[0.6, 1.2]
v_κ	OU speed reversion rate	[0.6, 1.4]
v_σ	OU speed noise intensity	[0.15, 0.45]
$v_{\min}$	Minimum cloud speed [km/unit time]	0.0
A_{mean}	OU amplitude mean [pu/km]	[0.0002, 0.015]
A_κ	OU amplitude reversion rate	[0.2, 1.0]
A_σ	OU amplitude noise intensity	[0.00005, 0.002]
A_0	Initial amplitude [pu/km]	A_{mean}
λ_{kill}	Cloud kill rate [1/unit time]	[0.05, 0.25]
γ_{fade}	Fade decay rate	[0.5, 2.0]
W_0	Initial cloud width [km]	[0.4, 1.0]
w_μ	OU mean width [km]	[0.5, 1.2]
w_κ	OU width reversion rate	[0.5, 1.2]
w_σ	OU width noise intensity (log-scale)	[0.15, 0.35]

References

[1] P. K. Kundu, I. M. Cohen, and D. R. Dowling, *Fluid mechanics*. Academic press, 2015.

[2] R. R. Craig Jr and A. J. Kurdila, *Fundamentals of structural dynamics*. John Wiley & Sons, 2006.

[3] F. P. Beer, E. R. Johnston, J. T. DeWolf, and D. F. Mazurek, *Mechanics of Materials*, 6th ed. New York: McGraw-Hill Education, 2012, euler–Bernoulli beam equation example.

[4] A. Semlyen, "Analysis of disturbance propagation in power systems based on a homogeneous dynamic model," *IEEE Transactions on Power Apparatus and Systems*, no. 2, pp. 676–684, 1974.

[5] ——, "Effect of nonuniformity on the continuous representation of electromechanical dynamics in large power systems," *IEEE Power Engineering Review*, vol. 18, no. 5, pp. 60–61, 2002.

[6] J. S. Thorp, C. E. Seyler, and A. G. Phadke, "Electromechanical wave propagation in large electric power systems," *IEEE Transactions on Circuits and Systems I: Fundamental Theory and Applications*, vol. 45, no. 6, pp. 614–622, 1998.

[7] M. Parashar, J. S. Thorp, and C. E. Seyler, "Continuum modeling of electromechanical dynamics in large-scale power systems," *IEEE Transactions on Circuits and Systems I: Regular Papers*, vol. 51, no. 9, pp. 1848–1858, 2004.

[8] T. Li, G. Ledwich, Y. Mishra, and J. Chow, "Power system stability implications from electromechanical wave propagation," in *IEEE PES Asia-Pacific Power and Energy Engineering Conference*, 2015, pp. 1–5.

[9] G. Tzounas, I. Dassios, and F. Milano, "Frequency divider as a continuum," *IEEE Transactions on Power Systems*, vol. 37, no. 6, pp. 4970–4973, 2022.

[10] F. M. d. S. Monteiro, J. V. de Souza, and E. N. Asada, "Analytical method to estimate the steady-state voltage impact of non-utility distributed energy resources," *Electric Power Systems Research*, vol. 218, p. 109190, 2023.

[11] L. V. Strezoski, N. R. Vojnovic, V. C. Strezoski, P. M. Vidovic, M. D. Prica, and K. A. Loparo, "Modeling challenges and potential solutions for integration of emerging ders in dms applications: power flow and short-circuit analysis," *Journal of Modern Power Systems and Clean Energy*, vol. 7, no. 6, pp. 1365–1384, 2019.

[12] G. Fusco and M. Russo, "A decentralized approach for voltage control by multiple distributed energy resources," *IEEE Transactions on Smart Grid*, vol. 12, no. 4, pp. 3115–3127, 2021.

[13] W. Zhong, G. Tzounas, and F. Milano, "Improving the power system dynamic response through a combined voltage-frequency control of distributed energy resources," *IEEE Transactions on Power Systems*, vol. 37, no. 6, pp. 4375–4384, 2022.

[14] M. Chertkov, S. Backhaus, K. Turitsyn, V. Chernyak, and V. Lebedev, "Voltage collapse and ode approach to power flows: Analysis of a feeder line with static disorder in consumption/production," *arXiv preprint arXiv:1106.5003*, 2011.

[15] D. Wang, K. Turitsyn, and M. Chertkov, "DistFlow ODE: Modeling, analyzing and controlling long distribution feeder," in *IEEE Conference on Decision and Control (CDC)*. IEEE, 2012, pp. 5613–5618.

[16] N. Mizuta, Y. Susuki, Y. Ota, and A. Ishigame, "An ODE-based design of spatial charging/discharging patterns of in-vehicle batteries for provision of ancillary service," in *IEEE Conference on Control Technology and Applications*. IEEE, 2017, pp. 193–198.

[17] ——, "Synthesis of spatial charging/discharging patterns of in-vehicle batteries for provision of ancillary service and mitigation of voltage impact," *IEEE Systems Journal*, vol. 13, no. 3, pp. 3443–3453, 2019.

[18] C. Vournas, "Maximum power transfer in the presence of network resistance," *IEEE Transactions on Power Systems*, vol. 30, no. 5, pp. 2826–2827, 2014.

[19] T. Y. Na, *Computational methods in engineering boundary value problems*. Academic press, 1980, vol. 145.